Sadi, Toufik; Radevici, Ivan; Behaghel, Benoît; Oksanen, Jani

Prospects and requirements for thermophotonic waste heat energy harvesting

Published in:
Solar Energy Materials and Solar Cells

DOI:
10.1016/j.solmat.2022.111635

Published: 01/06/2022

Document Version
Publisher's PDF, also known as Version of record

Solar Energy Materials & Solar Cells 239 (2022) 111635

Contents lists available at ScienceDirect

Solar Energy Materials and Solar Cells

journal homepage: www.elsevier.com/locate/solmat

Prospects and requirements for thermophotonic waste heat energy harvesting

Toufik Sadi *, Ivan Radevici, Benoît Behaghel, Jani Oksanen

Engineered Nanosystems group, School of Science, Aalto University, P.O. Box 12200, 00076 AALTO, Finland

ARTICLE INFO

Keywords:
Thermophotonics
Electroluminescent cooling
Thermophotovoltaics
Light-emitting diodes

ABSTRACT

Thermophotovoltaic (TPV) power generators offer great possibilities for thermal energy conversion when thermal sources with temperatures nearing or exceeding 1000 K are available. While the power density of conventional TPV systems is generally determined by Planck's law in the far field, their fundamental performance is known to be dramatically affected by near field effects between the thermal emitter and the photovoltaic cell. Another potentially disruptive enhancement to the performance may be reached by transforming the thermal emitter to exploit electroluminescence. Taking advantage of an electroluminescent emitter as the source of radiation fundamentally alters the thermodynamics of the system. This allows boosting the achievable power densities by orders of magnitude, and also provides access to electroluminescent coolers, thermophotonic (TPX) heat pumps, and TPX power generation devices that can outperform both TPV and thermoelectric heat engines, especially at the low-grade waste heat (LGWH) temperature range (300–500 K) containing in total the majority of recoverable energy. In reality, functional TPX devices are yet to be demonstrated experimentally, due to several material and design bottlenecks. Here, we discuss the thermodynamics, ideal characteristics and advantages of TPX heat engines, and quantify how non-idealities such as non-radiative recombination, optical and resistive losses affect their performance. Our results suggest that, at LGWH temperatures, TPX heat engines start to outperform the best TPV systems when reaching quantum efficiencies of the order of 90%; beyond this threshold, TPX systems become increasingly efficient and powerful.

1. Introduction

Both thermophotovoltaics (TPV) and photovoltaics (PV) enable converting radiative energy to electricity using the photovoltaic effect. However, unlike PV which directly converts solar radiation into electricity, TPV generates electrical power from heat radiated by a general hot body. This means that TPV systems can be employed for solar energy conversion, using an intermediate heated object [1], as well as for waste heat energy recovery applications [2]. In the latter area, they are especially well suited for high-grade waste heat (HGWH) recovery involving thermal sources with temperatures of the order of 900 K or more. At present, TPV systems are witnessing a revival thanks to advances in high-temperature materials science, photonics, and growth and processing of III–V semiconductors. Especially, progress in TPV is also encouraged by advances in nanogap engineering, which enable leveraging near-field effects, allowing up to orders of magnitude improvement in the photon flux from the hot body to the PV cell [3,4].

In general, waste heat released to the environment by global infrastructure is often classified into three categories: HGWH (>900 K), medium-grade waste heat (MGWH: ~ 500–900 K) and low-grade waste heat (LGWH: <500 K) [5]. Activities on waste heat recovery have largely focused on the upper MGWH and HGWH ranges, due to the technically more straightforward conversion by TPV. Considering that LGWH sources are estimated to contain in total more recoverable energy than the other waste heat sources combined [5,6], realizing LGHW conversion technology can be of great impact to the green economy. A possible pathway to accessing these low temperature energy streams can be envisioned through thermophotonics (TPX), that was originally proposed and previously studied for solar energy harvesting using an intermediate solar heated light emitter [7,8]. It generalized the TPV concept by allowing radiation from the emitter to be enhanced by an internal electronic excitation, e.g. by using a biased semiconductor light-emitting diode (LED) as the emitter. TPX systems deriving from this early concept have recently been identified as a plausible route for optical cooling [9–11] as well as LGWH recovery [5]. The basic concept of a thermophotonic device is illustrated in Fig. 1(a), showing a schematic of a TPX heat engine. These emerging possibilities are based

* Corresponding author.
E-mail address: toufik.sadi@aalto.fi (T. Sadi).

https://doi.org/10.1016/j.solmat.2022.111635
Received 10 July 2021; Received in revised form 13 January 2022; Accepted 31 January 2022
Available online 19 February 2022

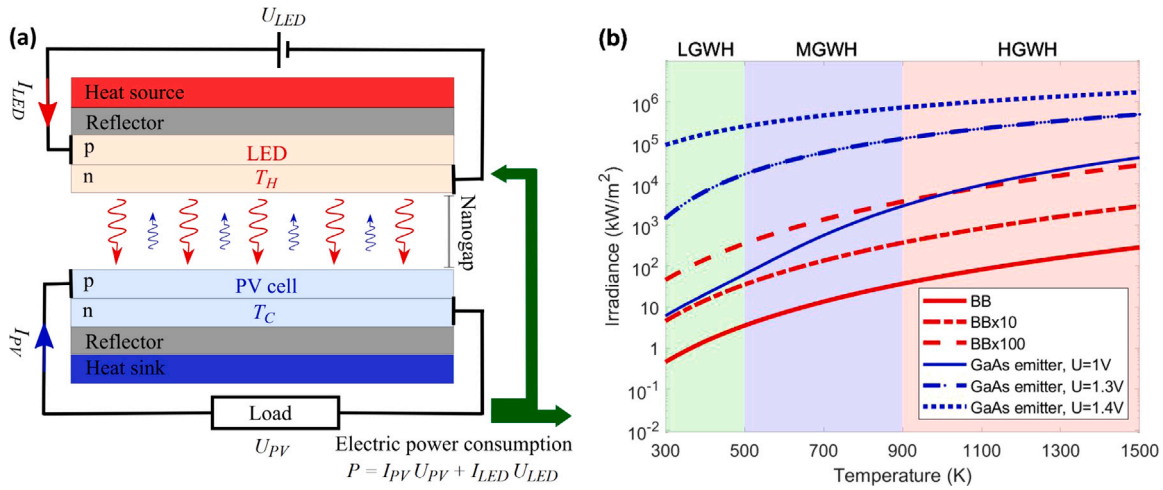

Fig. 1. (a) A schematic representation of a TPX heat engine, formed by a heated LED (at temperature $T_H > 300$ K) coupled to a PV device (typically at $T_C = 300$ K). Applying appropriate LED and PV device biases (U_{LED} and U_{PV}) produces electric currents (I_{LED} and I_{PV}) leading to a net power consumption $P = I_{PV}U_{PV} + I_{LED}U_{LED}$, with a negative P indicating net power generation; throughout the paper, we assign a positive (negative) current for the case when current is injected into (extracted from) the emitter/absorber, to highlight the symmetry between emitter and absorber. Photon symbols indicate the (red) LED-to-PV and (blue) PV-to-LED optical energy fluxes. (b) Radiation intensity as a function of T from three systems: (i) a black body (BB) emitter, (ii) [tenfold (×10) and hundredfold (×100)] enhanced black body radiation (as achieved e.g. using near field effects), and (iii) a GaAs emitter biased using three (low to high) voltages (1 V, 1.3 V and 1.4 V), and assuming emissivity $\varepsilon(\hbar\omega) = 1$. The GaAs bandgap photon energy is fixed to ~1.42 eV. (For interpretation of the references to color in this figure legend, the reader is referred to the web version of this article.)

on harnessing the thermodynamics of electroluminescence of LEDs to enhance the radiation intensity and consequently also PV energy production. Directly following from the related fundamental thermodynamics at play, the radiation from a heated electroluminescent emitter can exceed the corresponding black body values by several orders of magnitude; this is illustrated in 1(b), comparing the radiation intensity of a black body and a biased GaAs emitter as a function of temperature. The enhancement observed in the figure will be further shown to dramatically improve the LGWH energy collection performance, and to enable increasing the power generation density and efficiency to levels that are out of reach for TPV systems, at the abundant waste heat temperatures in the LGWH range of 300–500 K.

Historically, the concretization of TPX devices has faced two general challenges: (i) achieving a high enough optical energy transfer efficiency between the emitter (LED) and the absorber (PV cell), and (ii) reaching sufficiently large light emission efficiencies in the LED. Despite the earlier challenges, however, there are many indications that they can be overcome by combining recent advances from related technologies. For instance, our recent results [10,11] indicate that an above-unity wall-plug efficiency (WPE) for light emission is already possible with III–V compound semiconductors under optimal conditions. In addition, thermal insulators needed to enable strong near-field optical coupling between the LED and the PV cell have been previously devised, using micro-electromechanical system (MEMS) tubular spacers [12] and piezoelectrically actuated control stages [3]. In practice, however, it is presently not established what performance parameters are required from the technical solutions to allow practical devices. While it is expected that the actual TPX bottlenecks are primarily technological, involving e.g. minimizing device resistances and optical losses, establishing the parameter space allowing technical and fundamental demonstrations is an important step towards realizing TPX devices.

In this paper, we present a parametrized thermodynamic model describing the energy flows in generic TPX and TPV heat engine arrangements as a function of the most relevant loss parameters. The results (i) highlight the possible advantages of using TPX over TPV systems at LGWH temperatures, (ii) motivate the targeting of certain wide bandgap materials, and (iii) quantify the adverse impact of non-radiative recombination, optical and resistive losses, allowing to provide information on the required design parameters enabling functioning TPX heat engines.

2. The mathematical model

2.1. Radiation description

An ideal black body absorbs all electromagnetic radiation incident on it. It also reciprocally emits thermal radiation in a continuous spectrum as determined by its temperature. In real life, emitters are imperfect and absorb only part of the incident energy upon them. Such deviations to normal black body characteristics arise from various factors, such as the optical environment, excitation, and material properties and structure, and are quantified using the spectral emissivity parameter $\varepsilon(\hbar\omega)$, varying from 0 (perfect reflection) to 1 (perfect absorption). The emissivity directly reflects the absorptivity, and the spectral irradiance of luminescence $\mathcal{E}$ can be written, with respect to the photon energy $\hbar\omega$, as follows [13]:

$$\mathcal{E}(\hbar\omega, U, T) = \hbar\omega\ \varepsilon(\hbar\omega)\ \rho(\hbar\omega, n_r)\ f_{BE}(\hbar\omega, U, T), \tag{1}$$

where $\rho(\hbar\omega, n_r)$ is the optical density of states, and n_r is the refractive index of the media transporting the light. Here, $\hbar$ and ω are the reduced Planck's constant and the angular photon frequency, respectively. Also, $f_{BE}(\hbar\omega, U, T)$ is the generalized (bias-dependent) Bose–Einstein distribution [13], where U is the voltage quantifying the electronic excitation (e.g. the quasi-Fermi level separation between the conduction and valence bands of an excited semiconductor emitter) and T is the emitter temperature. More quantitatively, ρ and f_{BE} are given by

$$\rho(\hbar\omega, n_r) = \frac{(\hbar\omega)^2 n_r^2}{4\pi^2\hbar^3 c_0^2}, \tag{2}$$

$$f_{BE}(\hbar\omega, U, T) = \frac{1}{\exp[(\hbar\omega - qU)/k_B T] - 1}, \tag{3}$$

with c_0 being the speed of light in vacuum. The modified Bose–Einstein distribution f_{BE} given by Eq. (3) allows differentiating between the thermal ($U = 0$) and super-thermal ($E_g > U > 0$) radiation, by introducing a chemical potential U for the photons emitted by band-to-band recombination with energy larger than the emitter bandgap energy E_g. This formulation extends the Planck's law for thermal radiation, allowing the expression of electrically enhanced radiation as a function of the real temperature and the quasi-Fermi level separation. While the formulation above does not fully include the impact of certain non-idealities, such as resonant loss factors, nonlinearities, or stimulated emission, it already provides a good first order description of the fundamentals.

2.2. Irradiance of an object

Following from Eq. (1), the irradiance $\mathcal{I}$ of an object can be calculated from

$$\mathcal{I}(U,T,E_g) = \int_{E_g}^{\infty} \mathcal{E}(\hbar\omega,U,T)d\hbar\omega + \int_{0}^{E_g} \mathcal{E}(\hbar\omega,0,T)d\hbar\omega. \quad (4)$$

In Eq. (4), the emission above and below the bandgap are separately presented; the former term accounts for the spontaneous emission associated with above the bandgap ($\hbar\omega \geq E_g$) photons benefiting from the application of the electrical energy in the form of a bias, while the latter term is the emission associated with the below the bandgap ($\hbar\omega < E_g$) photons corresponding to conventional thermal radiation. The essential and only difference to pure thermal radiation in Eqs. (1) and (4) is that the electrical excitation U modifies the emission rate above the bandgap through its contribution to the distribution function F and thereby strongly enhances the spontaneous emission rate of high energy photons.

The formulation presented above directly implies an enhancement of the emission power that was illustrated in Fig. 1(b), comparing the radiation intensity for black body and electrically-biased GaAs emitters obtained using Eq. (4). Indeed, the mere application of a relatively low bias (1 V) already increases the intensity by at least tenfold in the LGWH temperature range. Applying a moderate bias of 1.3 V (still 0.12 V below the bandgap bias) provides at least a three orders of magnitude improvement with respect to the black body case, far more than what can be achieved from e.g. a hundredfold near-field enhancement. Applying a near-the-bandgap bias (1.4 V) leads to more than five orders of magnitude enhancement in the LGWH range; even at higher temperatures (e.g. at 1500 K), a four orders of magnitude enhancement is observed.

2.3. Photon fluxes and electric currents

The photon flux F_i emitted by an object i (either the 'hot' object (the LED/emitter) or the 'cold' object (PV cell/absorber) forming the TPX device), above its bandgap as a result of radiative recombination of electrons and holes, is given by

$$F_i = \int_{E_g}^{\infty} \frac{1}{\hbar\omega}\mathcal{E}(\hbar\omega,U_i^0,T_i)d\hbar\omega, \quad (5)$$

where U_i^0 and T_i represent the voltage corresponding to the chemical potential (i.e. the quasi-Fermi level separation) and temperature of the object, respectively. As such, the radiative current density through the object can be written as

$$J_r^i = \frac{qF_i}{\eta_{exe}^i}, \quad (6)$$

where η_{exe}^i parameterizes the photon extraction/removal efficiency (corresponding approximately to light extraction efficiency and photon escape probability in the LED and PV terminologies, respectively) from the object. The total recombination current density can then be parametrized as

$$J_i^{\text{dark}} = J_r^i + J_{NR}^i = \frac{J_r^i}{\eta_{IQE}^i} = \frac{qF_i}{\eta_{EQE}^i}, \quad (7)$$

where J_{NR}^i is the non-radiative current, originating from Shockley–Read–Hall, Auger or other non-radiative electron–hole recombination processes, and η_{IQE}^i is the internal quantum efficiency (IQE, also known as the internal luminescence efficiency). Here, the current is also written as a function of the object's external quantum efficiency (EQE, also known as the external luminescence efficiency) using the relation $\eta_{EQE} = \eta_{exe}\eta_{IQE}$ [14]. The EQE therefore accounts for all types of quantum losses present in real emitters, whether they result from photon absorption anywhere in the structure, nonradiative recombination or any other mechanisms effectively leading to the loss of injected energy quanta without producing a photon that is extracted outside the emitter.

Energy recycling in a TPX heat engine arrangement coupling two electrically biased objects, as illustrated in Fig. 1(a), profoundly affects the net energy flow and the photon flux into the objects. (While both TPV and TPX systems can also inherently recycle optical energy through reflections and re-emission, the term 'energy recycling' used here refers to the recycling of the electricity generated by the PV cell.) In a TPX system, where the object i is coupled to another object j, the net current density is given by

$$J_i = J_i^{\text{dark}} - J_i^L = \frac{qF_i}{\eta_{EQE}^i} - \eta_{CQE}^{ji}\, qF_j, \quad (8)$$

where J_i^L is the current in object i due to the absorption of photons from object j, and η_{CQE}^{ji} is the coupling quantum efficiency (CQE) of the light from object j to object i [15].

Ideally, the above bandgap emissivity in Eq. (4) would be spectrally optimized to balance the performance in terms of the power density and efficiency, while the effective emissivity below the bandgap should be minimized e.g. by using high reflectivity back surface mirrors on the absorber as done by the TPV community [16,17], and also by minimizing sub-bandgap absorption. In this work, however, we will primarily use the emissivity value of unity throughout the spectrum for simplicity, since it will not notably affect our main conclusions, even if it is expected to overestimate the sub-bandgap loss.

2.4. Output power and efficiency

Since Fig. 1(a) is only included for illustrative purposes, the net power consumption is expressed only as a function of the LED and PV externally applied biases (U_{LED} and U_{PV}, respectively) and the produced electric currents (I_{LED} and I_{PV}, respectively), without describing losses; here, the LED (PV) current is simply the product of LED (PV) current density J_{LED} (J_{PV}) and the device area. In reality, and from the relationships above, it follows that the electrical power P per unit area needed to drive a TPX system, consisting of the emitter (LED) and the absorber (PV cell), is given by

$$P = \underbrace{U_{LED}J_{LED} + J_{LED}^2 R_{LED}}_{P_{LED}} + \underbrace{U_{PV}J_{PV} + J_{PV}^2 R_{PV}}_{P_{PV}}, \quad (9)$$

where R_{LED} (R_{PV}) is the specific resistance for a unit area of the emitter (absorber). In device terms, both R_{LED} and R_{PV} may include contact and spreading resistances. Eq. (9) separately highlights the power consumed by the emitter (P_{LED}) and absorber (P_{PV}). With the chosen sign convention, a negative P implies power production, with a negative current implying current generation. The external voltage U_i of element i ($i \in$ {LED,PV}) additionally relates to the resistance R_i and the internal electrical excitation U_i^0 through

$$U_i = U_i^0 + J_i\, R_i. \quad (10)$$

Here, positive currents (e.g. in the LED) imply that the internal excitation is smaller than the external excitation, and negative currents (e.g. in the PV cell) imply that the external excitation is smaller than the internal excitation. Finally, the net heat flux Q transferred from the LED to the PV cell is given by

$$Q = \mathcal{I}(U_{LED}^0,T_H,E_g) - \mathcal{I}(U_{PV}^0,T_C,E_g) - P_{LED}, \quad (11)$$

i.e. it is obtained from energy conservation as the difference between the net emitted optical power and the electrical power consumed by the LED. Here, T_H and T_C are the LED and PV temperatures, respectively. Noting the sign convention, it follows that the efficiency η of a thermophotonic heat engine is given by

$$\eta = -\frac{P}{Q}. \quad (12)$$

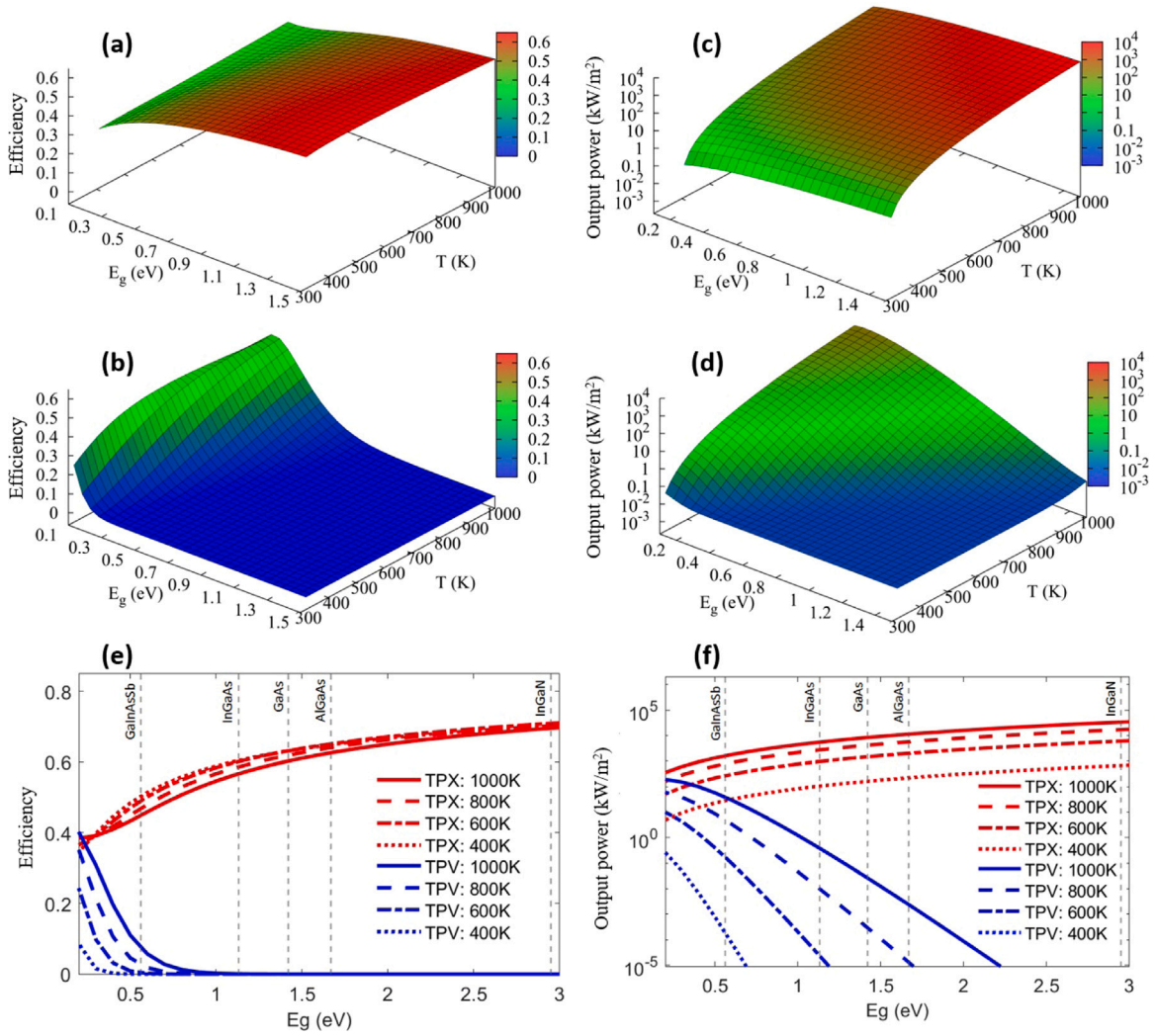

Fig. 2. The maximum efficiency of the (a) TPX and (b) TPV power generators, as a function of emitter bandgap and temperature. The maximum output power (in kW/m^2) for the (c) TPX and (d) TPV power generators, as a function of emitter bandgap and temperature; for convenient representation, power densities below 10^{-3} kW/m^2 are shown in blue. One dimensional profiles of the maximum (e) efficiency and (f) output power as a function of the bandgap, for various temperatures, for both TPX and TPV generators; for illustrative purposes, the bandgap of selected industrially-interesting materials are marked in both subfigures. (For interpretation of the references to color in this figure legend, the reader is referred to the web version of this article.)

In the analysis carried out below, we will present efficiencies as normalized by the Carnot limit of a heat engine, given by

$$\eta_{Carnot} = \frac{T_H - T_C}{T_H}. \tag{13}$$

In the calculations, T_C is set to 300 K. The emissivity as well as the (LED-to-PV and PV-to-LED) CQE values are assumed to take the idealized value of unity, unless stated otherwise. Also, in our analysis, we assume that all of the transport takes place in an effectively homogeneous space that has a refractive index of $n_r = 3.65$ (corresponding to GaAs at its bandgap wavelength [18]), as in the double diode structures (DDSs) studied by the authors [10] and as in near field devices [3]. The studied TPX devices are therefore assumed to be separated by a perfect vacuum nanogap or a hypothetical transparent and lossless material with an effective refractive index matched with the semiconductor materials.

3. Results and discussions

3.1. Comparison of TPX and TPV configurations

To demonstrate how the large power density seen in Fig. 1(b) reflects device performance, we show in Fig. 2 the maximum obtainable efficiency (normalized to the Carnot efficiency) and output power (in kW/m^2) as a function of temperature and bandgap, for idealized TPX and TPV systems (i.e. for unity $\epsilon(\hbar\omega)$, η_{exe} and η_{CQE}, and negligible non-radiative recombination, ohmic dissipation and resistive losses). The optimized values are obtained by finding the emitter and absorber biases that maximize the efficiency or power, respectively. The calculations further assume the same emitter and absorber bandgaps and refractive index ($n_r = 3.65$). Specifically, Figs. 2(a) and (b) show the maximum efficiency of TPX and TPV systems, respectively, as a function of the bandgap and emitter temperature. Figs. 2(c) and (d) show the maximum power from TPX and TPV systems, accordingly, also as a function of both parameters, while Figs. 2(e) and (f) show the corresponding one dimensional profiles of the efficiency and power density, for more accurate quantitative visualization, as a function of the bandgap, for selected temperatures. It can be seen from Figs. 2(a) and (e) that the efficiency of an idealized TPX configuration increases with the bandgap, from approximately 35% at $E_g = 0.2$ eV to 70% at $E_g = 3$ eV. Also, even for the wide temperature range considered here, the dependence of efficiency on temperature is weak. In contrast, in an idealized TPV system [Figs. 2(b) and (e)], we observe a strong dependence of efficiency on the bandgap, with the highest values being obtainable at low bandgaps (below 0.6 eV). The dependence on

temperature is stronger at low bandgaps, ranging from almost 0% at 300 K, to 60% at the high temperature of 1000 K. For the output power, Figs. 2(c) and (f) show how the maximum values for the TPX system increase substantially with both the bandgap and temperature, reaching e.g. the value of approximately 1700 kW/m^2 at E_g = 1.5 eV and T = 600 K. The power from the TPV system [Figs. 2(d) and (f)], on the other hand, decreases dramatically as the bandgap increases or the temperature decreases, giving values comparable to TPX only at very small bandgaps and very high temperatures; indeed, the peak power of ~190 kW/m^2 is reached at the lowest considered bandgap of 0.2 eV and the highest considered temperature of 1000 K. Even then, the value is almost one order of magnitude smaller than the peak value reached in the TPX system, highlighting in quantitative terms the advantage of using an LED as a superthermal emitter.

The vertical lines in Figs. 2(e) and (f) highlight the bandgaps corresponding to five industrially-interesting materials that may be considered to have potential for thermophotonics or thermophotovoltaics: GaAs [10], $In_{0.2}Ga_{0.8}N$ [19,20], $Al_{0.2}Ga_{0.8}As$ [5], $In_{0.15}Ga_{0.85}As$ [21] and GaInAsSb [22]. In general, larger bandgaps are more beneficial in TPX devices, as they provide access to larger optical density of states, although such benefit can be lost if the emitter and absorber are separated by non-index matched materials. While GaAs – preferred so far in our electroluminescent cooling (ELC) experiments [10] – provides a good TPX performance, using a higher bandgap related alloy such as $Al_{0.2}Ga_{0.8}As$ could provide improvements in both the efficiency and power but, more significantly, can allow tuning the bandgap to match the emission and absorption spectra of the components, if necessary. The eventual need for bandgap matching will, however, depend on several factors, such as the temperature difference and the effectiveness of state-of-the-art photon rejection solutions in preventing the energy loss due to the photons that are not absorbed by the PV cell (see e.g. Ref. [23]). In theory, III-N can provide the highest efficiencies (up to ~10% higher than the maximum obtained from any other studied material) and considerably more power as compared to GaAs (e.g. 3250 kW/m^2 for InGaN as compared to 1500 kW/m^2 for GaAs, at 600 K). However, realistic III-N based LEDs typically incorporate thinner active regions [24] and involve more complex processing as compared to III-As based LEDs, and hence accessing the output power advantage can require more work in practice. Due to the smaller efficiency and output power, as well as generally high non-radiative recombination values, it is expected that using narrow bandgap materials such as GaInAsSb for thermophotonics will be less attractive. Also, while the efficiency of the InGaAs system is almost similar to that of the GaAs case (e.g. a maximum of 60% for InGaAs as compared to 63% for GaAs, at 600 K), it would in theory already induce a significant disadvantage in the output power (with the maximum dropping from 1500 kW/m^2 in GaAs to 900 kW/m^2 in InGaAs, at 600 K).

It is noteworthy that the incorporation of perfect back-surface reflectors (BSRs) with a reflectivity nearing unity for sub-bandgap photon energies [16,17] can provide even higher efficiencies for both TPV and TPX power generation. This is illustrated in Fig. 3 showing the variation of the efficiency for both TPX and TPV systems, at T = 600 K, when the emissivity below the bandgap in Eq. (1) is set to values 0, 0.001, 0.1 and 1; this approximately corresponds to the situation where the absorber exhibits complete sub-bandgap transparency and is terminated by a BSR with a reflectivity of 100, 99.9, 90 and 0% for the sub-bandgap wavelengths, respectively. When the sub-bandgap losses are fully eliminated, both the TPX and TPV efficiencies become equal and notably larger than in the unity emissivity case presented in Fig. 2. For larger bandgap materials, the efficiency of the TPV system nevertheless quickly decreases if any sub-bandgap absorption or mirror losses are present: e.g. even with a BSR reflectivity of 99.9%, the efficiency of the TPV system drops from the peak value of 80% to about 10% at the bandgap of 0.8 eV. For TPX, the sub-bandgap loss also reduces the efficiency but, in contrast to the TPV system, the efficiency keeps increasing with larger bandgaps and exceeds 50% of the Carnot limit over a wide range even when all the sub-bandgap photons are lost. Despite these changes in the efficiency, however, the output power of both the TPV and TPX systems remains essentially independent of the sub-bandgap loss.

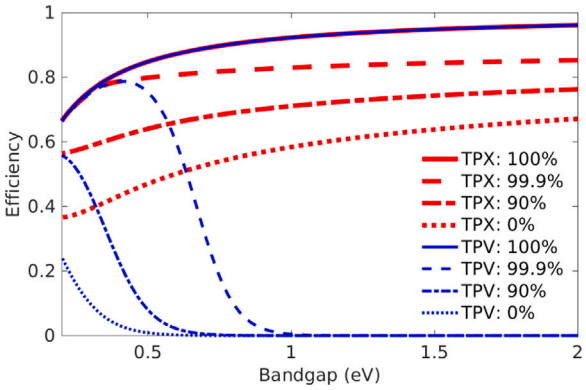

Fig. 3. The variation of the Carnot-scaled efficiency for both TPX (red lines) and TPV (blue lines) systems, for the BSR reflectivities of 0, 90, 99.9 and 100%, at T = 600 K. In the complete absence of any sub-bandgap losses, both systems are equally efficient and approach Carnot efficiency at large bandgaps, but only the TPX system maintains high efficiency at larger bandgaps when any sub-bandgap losses are present. (For interpretation of the references to color in this figure legend, the reader is referred to the web version of this article.)

3.2. Impact of non-idealities

Understanding the exact limitations of non-idealities in demonstrating thermophotonic heat engines is crucial to their development. While effects such as non-radiative recombination, optical extraction and resistive losses, are all known challenges for TPX applications [5,11,25,26], a quantitative understanding of their concrete impact on heat engine performance is necessary to develop and benchmark the technical solutions. Few previous works have touched this issue on the technology-agnostic level. In a structure-specific study, Zhao et al. [5] analyzed the impact of LED, PV cell and nanogap thicknesses and mirror reflectivity on the performance of a TPX heat engine device incorporating highly reflective back mirrors. Also, Tobias et al. [8] looked at the impact of non-idealities, such as non-radiative recombination, on the efficiency of solar thermophotonic converters. Additionally, the present authors have discussed how non-radiative recombination and optical losses are general bottlenecks in observing ELC in a TPX cooler prototype [11,26]. Here, in contrast, we carry out a parametric study mapping out the simultaneous impact of these factors as well as device resistances, to provide practical criteria for the design of TPX heat engines, primarily applying the developed models with GaAs active regions in mind.

To introduce the impact of non-radiative recombination and non-unity extraction efficiencies, Figs. 4(a) and (b) show respectively the maximum obtainable efficiency and output power, as a function of temperature, for selected emitter and absorber EQEs (with $\eta_{EQE}^{LED} = \eta_{EQE}^{PV}$), assuming negligible ohmic dissipation and resistances in the system. As can be observed, the peak values for the efficiency drop quickly, from 63% to 18% when the EQE is reduced from 100% to just 95%. The impact on the output power is even more dramatic, dropping from ~1500 kW/m^2 at η_{EQE} = 100% to ~25 kW/m^2 at η_{EQE} = 95%. This highlights well the main challenge of thermophotonics, requiring very efficient materials and device designs, but luckily, modern compound semiconductors such as GaAs already enable very high internal quantum efficiencies due to their small SRH [27–29] and Auger [30] recombination constants, making radiative recombination the dominant process at least at room temperature and low temperatures. This leads to IQEs exceeding 99% [27,31], although the IQE is

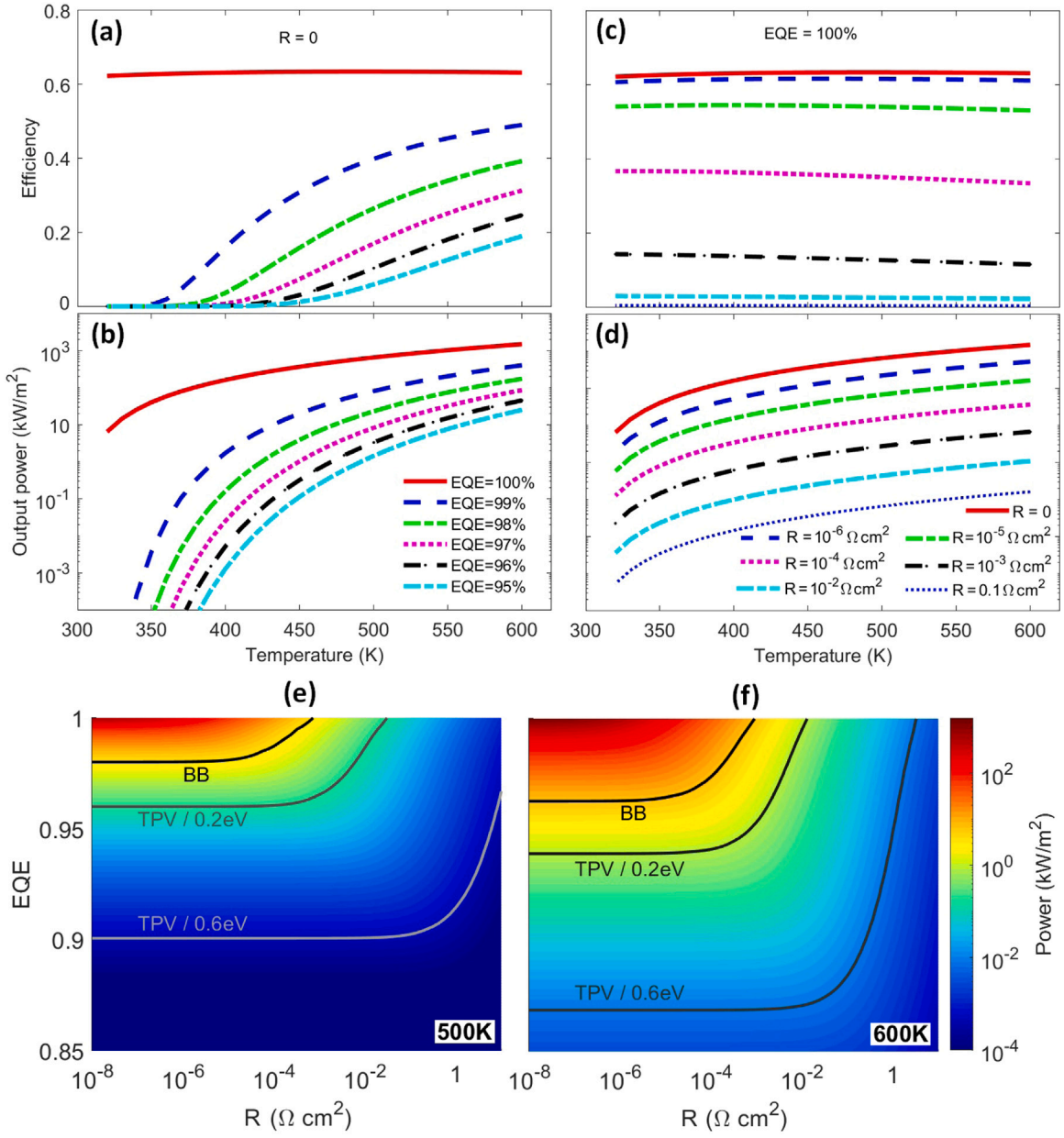

Fig. 4. The maximum obtainable (a) efficiency and (b) output power, as a function of temperature, for selected emitter and absorber EQEs (with $\eta_{EQE}^{LED} = \eta_{EQE}^{PV}$), assuming a negligible resistance. The maximum (c) efficiency and (d) output power as a function of temperature, for various emitter and absorber resistances ($R = R_{LED} = R_{PV}$), assuming $\eta_{EQE}^{LED} = \eta_{EQE}^{PV} = 1$. The maximum output power as a function of both the emitter and absorber's EQE ($\eta_{EQE} = \eta_{EQE}^{LED} = \eta_{EQE}^{PV}$) and total resistance ($R = R_{LED} = R_{PV}$), for two temperatures: (e) 500 K and (f) 600 K; here, we also show the contours corresponding to (i) the radiating power from a black body (BB) object, and the power that can be generated from the BB by an ideal TPV system with (ii) 0.2 eV and (iii) 0.6 eV absorber bandgaps, at the corresponding temperature; the contours directly follow from calculating the electric output power of the TPV cell, from the irradiance absorbed by the PV cell.

expected to drop at large temperatures. In addition, adopting better device designs can produce near-unity light extraction and external quantum efficiencies [32], most likely enabling the efficiencies needed to access TPX power generation.

Figs. 4(c) and (d) show respectively the maximum obtainable efficiency and output power as a function of temperature, for various emitter and absorber resistances ($R = R_{LED} = R_{PV}$), assuming unity external quantum efficiency ($\eta_{EQE}^{LED} = \eta_{EQE}^{PV} = 1$). As can be seen, the peak value for the efficiency drops in a visible fashion, from 63% to 62%, 55%, 37% and 14%, for a resistance of 10^{-6}, 10^{-5}, 10^{-4} and 10^{-3} Ω cm^2, respectively. A more visible effect is observed in the output power, dropping from 1500 kW/m^2 to 530, 165, 37 and 7 kW/m^2, for the same resistances of 10^{-6}, 10^{-5}, 10^{-4} and 10^{-3}Ω cm^2, respectively. Such results emphasize the importance of high quality contacts with very small interface resistances, and device designs with efficient current spreading characteristics using e.g. novel current injection techniques [33].

Finally, to visualize the impact of quantum efficiencies and resistive losses on the performance of a TPX heat engine loosely based on a material corresponding to GaAs (in terms of the bandgap and refractive index), we show in Fig. 4(e) and (f) the optimal output power as a function of the external quantum efficiency ($\eta_{EQE} = \eta_{EQE}^{LED} = \eta_{EQE}^{PV}$) and resistance ($R = R_{LED} = R_{PV}$), for the temperatures of 500 K and 600 K, respectively. In these maps, we also show the contours corresponding to (i) the radiating power from a black body (BB) object, and the power corresponding to the BB case multiplied by the (optimal) absolute efficiency from the TPV system with (ii) 0.2 eV and (iii) 0.6 eV absorber bandgaps, at the corresponding temperature. As a note, the

TPV system absolute efficiencies are respectively 5% (12%) and 0.01% (0.11%) for 0.2 eV and 0.6 eV bandgaps, at 500 K (600 K). As can be seen, the advantage of the TPX heat engine, over e.g. the ideal recovery of the black body emission, is maintained when the specific device resistance is kept below the 10^{-4} Ωcm^2 level, and the extraction efficiency losses do not exceed ~4% for $T_H = 500$ K and ~7% for $T_H = 600$ K. For proof of concept and first demonstration purposes, resistances as high as 10^{-2} Ωcm^2 and EQEs as low as 90% can still allow the generation of easily observable power densities that are comparable with the power densities allowed by the idealized TPV configurations, of the order of $10^{-2} - 1$ kW/m^2.

For completeness, we have verified that, due to the large range of power densities reached by varying the bias, typical changes in the material emissivities (e.g. 30% for a relatively thin layer of GaAs) do not affect significantly the quantitative and qualitative conclusions made above on the effect of non-idealities. Indeed, while reduced emissivities result in a proportional reduction in the output power, the range of EQEs and resistances needed to generate significant output power (as compared to the BB or TPV cases) do not change dramatically. Additional calculations using reduced emissivities (down to 5%) for the thermally emitted ($\hbar\omega < E_g$) photons suggest that emissivity engineering could enable an additional 15% improvement in the maximum efficiency, without affecting the maximum generated power. Also, it is of note that the applied external biases needed to reach the indicated power levels corresponding to BB emission or TPV power generation remain relatively low, typically ranging from 65% to 85% of the bandgap bias. The optimal biases strongly depend on many factors including device resistance and EQE. For example, for the optimized efficiency of a GaAs TPX heat engine at the realistically useful T of 600K, and for an EQE of 99% and for the same R range as in Fig. 4(f), the LED (PV) optimal bias varies from ~40% (~70%) of E_g to a maximum of ~85% (~90%) of E_g. Typically, TPX optimal biases decrease at higher device resistances and lower EQEs, reflecting the decreasing output power. In the equivalent case for TPV, the biases also depend on the parameters; for example at the realistically useful T of 1000K, and for a bandgap and EQE of 0.2 eV and 99%, respectively, the PV optimal bias ranges from 73% to 77% of E_g.

4. Conclusions

In this paper, we discussed the potential advantages of thermophotonics starting from the generalized form of Planck's law for thermal radiation. Based on the developed model, the advantages of thermophotonic over thermophotovoltaic systems are most attractive at LGWH temperatures and can lead to substantially improved efficiencies and power densities. Parametrized calculations showing the effect of device non-idealities, such as non-radiative recombination, optical extraction and resistive losses, however, highlight the need for high quality materials, characterized by nearly negligible SRH and Auger recombination at the relevant power range as well as a low level of device resistances. Overall, the present parametrization allows gaining valuable insight into the tolerated level of system losses, and shows that functional TPX heat engines are becoming within reach with already existing technologies.

Declaration of competing interest

The authors declare that they have no known competing financial interests or personal relationships that could have appeared to influence the work reported in this paper.

Acknowledgments

We acknowledge funding from the Academy of Finland, and the European Research Council's Horizon 2020 research and innovation programme, within the framework of the projects iTPX (grant agreement No 638173) and TPX-Power (grant agreement No 951976). The calculations presented above were performed using computer resources provided by the Aalto University School of Science "Science-IT" project.

References

[1] Y. Wang, H. Liu, J. Zhu, Solar thermophotovoltaics: Progress, challenges, and opportunities, APL Mater. 7 (2019) 080906, http://dx.doi.org/10.1063/1.5114829.

[2] B. Zhao, K. Chen, S. Buddhiraju, G. Bhatt, M. Lipson, S. Fan, High-performance near-field thermophotovoltaics for waste heat recovery, Nano Energy 41 (2017) 344, http://dx.doi.org/10.1016/j.nanoen.2017.09.054.

[3] A. Fiorino, L. Zhu, R. Thompson, P. Reddy, E. Meyhofer, Nanogap near-field thermophotovoltaics, Nature Nanotechnol. 13 (2018) 806–811, http://dx.doi.org/10.1038/s41565-018-0172-5.

[4] C. Lucchesi, R. Vaillon, P.-O. Chapuis, Radiative heat transfer at the nanoscale: experimental trends and challenges, Nanoscale Horiz. 6 (2021) 201–208, http://dx.doi.org/10.1039/D0NH00609B.

[5] B. Zhao, P. Santhanam, K. Chen, S. Buddhiraju, S. Fan, Near-field thermophotonic systems for low-grade waste-heat recovery, Nano Lett. 18 (2018) 5224, http://dx.doi.org/10.1021/acs.nanolett.8b02184.

[6] I. Johnson, W.T. Choate, A. Davidson, Waste Heat Recovery. Technology and Opportunities in U.S. Industry, URL https://www.osti.gov/biblio/1218716-waste-heat-recovery-technology-opportunities-industry.

[7] N.-P. Harder, M.A. Green, Thermophotonics, Semicond. Sci. Technol. (2003) S270–S278, http://dx.doi.org/10.1088/0268-1242/18/5/319.

[8] I. Tobias, A. Luque, Ideal efficiency and potential of solar thermophotonic converters under optically and thermally concentrated power flux, IEEE Trans. Electron Devices 49 (11) (2002) 2024–2030, http://dx.doi.org/10.1109/TED.2002.804731.

[9] J. Oksanen, J. Tulkki, Thermophotonic heat pump–a theoretical model and numerical simulations, J. Appl. Phys. 107 (9) (2010) 093106–1–8, http://dx.doi.org/10.1063/1.3419716.

[10] I. Radevici, J. Tiira, T. Sadi, A. Ranta, M. Guina, J. Oksanen, Thermophotonic cooling in GaAs based light emitters, Appl. Phys. Lett. 114 (2019) 051101, http://dx.doi.org/10.1063/1.5064786.

[11] T. Sadi, I. Radevici, J. Oksanen, Thermophotonic cooling with light-emitting diodes, Nat. Photonics 14 (2020) 205–214, http://dx.doi.org/10.1038/s41566-020-0600-6.

[12] R.S. DiMatteo, P. Greiff, S.L. Finberg, K.A. Young-Waithe, M.M. Choy, C.G. Fonstad, Micron-gap ThermoPhotoVoltaics (MTPV), AIP Conf. Proc. 653 (2003) 232, http://dx.doi.org/10.1063/1.1539379.

[13] P. Würfel, The chemical potential of radiation, J. Phys. C: Solid State Phys. 15 (1982) 3967–3985.

[14] P. Kivisaari, L. Riuttanen, J. Oksanen, S. Suihkonen, M. Ali, H. Lipsanen, J. Tulkki, Electrical measurement of internal quantum efficiency and extraction efficiency of III-n light-emitting diodes, Appl. Phys. Lett. 101 (2) (2012) 021113, http://dx.doi.org/10.1063/1.4736565.

[15] A. Olsson, J. Tiira, M. Partanen, T. Hakkarainen, E. Koivusalo, A. Tukiainen, M. Guina, J. Oksanen, Optical energy transfer and loss mechanisms in coupled intracavity light emitters, IEEE Trans. Electron Devices 63 (9) (2016) 3567–3573, http://dx.doi.org/10.1109/TED.2016.2590461.

[16] T. Burger, C. Sempere, B. Roy-Layinde, A. Lenert, Present efficiencies and future opportunities in thermophotovoltaics, Joule 4 (2020) 1660–1680, http://dx.doi.org/10.1016/j.joule.2020.06.021.

[17] A. Datas, Ultra-high temperature thermal energy storage, transfer and conversion, Elsevier, 2020, http://dx.doi.org/10.1016/C2019-0-00964-8, Chapter 11 – Thermophotovoltaic energy conversion.

[18] D.E. Aspnes, S.M. Kelso, R.A. Logan, R. Bhat, Optical properties of $Al_xGa_{1-x}As$, J. Appl. Phys. 60 (1986) 754–767, http://dx.doi.org/10.1063/1.337426.

[19] S. Nakamura, M.R. Krames, History of gallium-nitride–based light-emitting diodes for illumination, Proc. IEEE 101 (10) (2013) 2211–2220, http://dx.doi.org/10.1109/JPROC.2013.2274929.

[20] S. Nakamura, background Story of the Invention of Efficient Blue InGaN light emitting diodes, URL https://www.nobelprize.org/prizes/physics/2014/nakamura/lecture/.

[21] N. Li, K. Han, W. Spratt, S. Bedell, J. Ott, M. Hopstaken, F. Libsch, Q. Li, D. Sadana, Ultra-low-power sub-photon-voltage high-efficiency light-emitting diodes, Nat. Photonics 13 (2019) 588–592, http://dx.doi.org/10.1038/s41566-019-0463-x.

[22] P. Santhanam, D.J. Gray, R.J. Ram, Thermoelectrically pumped light-emitting diodes operating above unity efficiency, Phys. Rev. Lett. 108 (9) (2012) 097403–1–5, http://dx.doi.org/10.1103/PhysRevLett.108.097403.

[23] D. Fan, T. Burger, S. McSherry, B. Lee, A. Lenert, S.R. Forrest, Near-perfect photon utilization in an air-bridge thermophotovoltaic cell, Nature 586 (2020) 237–241, http://dx.doi.org/10.1038/s41586-020-2717-7.

[24] J. Iveland, L. Martinelli, J. Peretti, J.S. Speck, C. Weisbuch, Direct measurement of Auger electrons emitted from a semiconductor light-emitting diode under electrical injection: Identification of the dominant mechanism for efficiency droop, Phys. Rev. Lett. 110 (2013) 177406, http://dx.doi.org/10.1103/PhysRevLett.110.177406.

[25] T. Patrick Xiao, K. Chen, P. Santhanam, S. Fan, E. Yablonovitch, Electroluminescent refrigeration by ultra-efficient GaAs light-emitting diodes, J. Appl. Phys. 123 (17) (2018) 173104–1–15, http://dx.doi.org/10.1063/1.5019764.

[26] T. Sadi, I. Radevici, P. Kivisaari, J. Oksanen, Electroluminescent cooling in III-v intracavity diodes: Efficiency bottlenecks, IEEE Trans. Electron Devices 66 (2019) 2651–2656, http://dx.doi.org/10.1109/TED.2019.2910219.

[27] D.A. Bender, J.G. Cederberg, C. Wang, M. Sheik-Bahae, Development of high quantum efficiency gaas/gainp double heterostructures for laser cooling, Appl. Phys. Lett. 102 (25) (2013) 252102, http://dx.doi.org/10.1063/1.4811759.

[28] G.D. Gilliland, D.J. Wolford, T.F. Kuech, J.A. Bradley, H.P. Hjalmarson, Minority-carrier recombination kinetics and transport in surface-free gaAs/Al_xGa_{1-x}As double heterostructures, J. Appl. Phys. 73 (1993) 8386–8396, http://dx.doi.org/10.1063/1.353407.

[29] R.J. Nelson, R.G. Sobers, Minority-carrier lifetimes and internal quantum efficiency of surface-free GaAs, J. Appl. Phys. 49 (1978) 6103, http://dx.doi.org/10.1063/1.324530.

[30] U. Strauss, W.W. Rühle, K. Köhler, Auger recombination in intrinsic GaAs, Appl. Phys. Lett. 62 (1993) 55–57, http://dx.doi.org/10.1063/1.108817.

[31] I. Schnitzer, E. Yablonovitch, C. Caneau, T.J. Gmitter, Ultrahigh spontaneous emission quantum efficiency, 99.7% internally and 72% externally, from AlGaAs/GaAs/AlGaAs double heterostructures, Appl. Phys. Lett. 62 (2) (1993) 131–133, http://dx.doi.org/10.1063/1.109348.

[32] M. Sheik-Bahae, R.I. Epstein, Optical refrigeration, Nat. Photonics 1 (12) (2007) 693–699, http://dx.doi.org/10.1038/nphoton.2007.244.

[33] A. Myllynen, T. Sadi, J. Oksanen, Current spreading in back-contacted GaInP/GaAs light-emitting diodes, IEEE Trans. Electron Devices 67 (3) (2020) 1027–1033, http://dx.doi.org/10.1109/TED.2020.2964662.